J. Fluid Mech. (1980), *vol.* 101, *part* 1, *pp.* 53–63
Printed in Great Britain

Vertical slender jets

By JAMES F. GEER
Department of Systems Science, S.U.N.Y. – Binghamton
AND JOHN C. STRIKWERDA
Institute for Computer Applications in Science and Engineering

(Received 7 November 1979 and in revised form 10 March 1980)

The shape of a vertical slender jet of fluid falling steadily under the force of gravity is studied. The problem is formulated as a nonlinear free boundary-value problem for the potential. Surface tension effects are neglected. The use of perturbation expansions results in a system of equations that can be solved by an efficient numerical procedure. Computations were made for jets issuing from orifices in various shapes including an ellipse, a rectangle, and an equilateral triangle. Computational results are presented illustrating the propagation of discontinuities and the formation of thin sheets of fluid.

1. Introduction

We wish to study the steady, three-dimensional potential flow of a slender jet of fluid falling vertically in the presence of gravity. Our primary interest is to determine the shape of the free surface of the jet, given the cross-sectional shape and velocity profile of the jet at a particular height (e.g. at an orifice from which the jet emanates). Surface tension and viscous effects are neglected.

The two-dimensional version of this problem (e.g. a thin sheet of water falling from a long slit in a container) has been studied by several investigators (see Keller & Geer 1973 and Geer & Keller 1979 and the references cited therein). In two dimensions, a rather straightforward perturbation analysis, based upon the slenderness ratio of the stream, leads to a sequence of problems which can be solved by standard methods of analysis (e.g. the numerical integration of some nonlinear ordinary differential equations together with methods from complex variable theory). In three dimensions (e.g. a jet of water falling from an elliptical orifice) the problem is considerably more difficult to analyse. The mathematical formulation of the problem leads to a fully three-dimensional, nonlinear boundary value problem for Laplace's equation, for which the boundary of the flow is also unknown. For the case of a slender jet, however, Tuck (1976) and Geer (1977*a*, *b*) derived equations to describe the first approximation to the cross-sectional shape and velocities of the jet. The problem of determining the shape is thus reduced to solving a nonlinear two-dimensional problem in the cross-sectional plane of the jet. Both Tuck and Geer gave an exact solution to this problem, namely, a jet with an elliptical cross-sectional shape. (See also Green 1977 for a one-dimensional analysis of jets with elliptical cross-sections.) To date no other exact solutions have been found.

0022-1120/80/4580-2410 $02.00

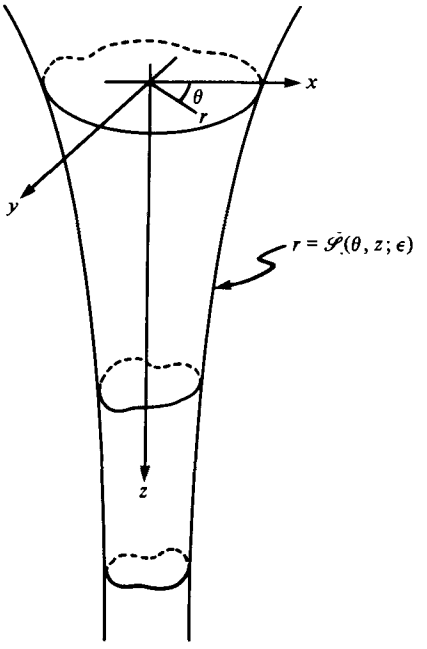

FIGURE 1. Sketch of a vertical slender jet, with an indication of the co-ordinate system. The locus of centroids of the cross-sections of the jet form a straight line (in the direction of gravity), which we choose to be the z axis. Then r, θ and z form the usual cylindrical co-ordinate system, where θ is measured from any convenient plane through the z axis. The free surface of the jet is denoted by $r = \mathscr{S}(\theta, z; \epsilon)$.

The purpose of this work is to present the results of solving numerically the associated nonlinear free boundary-value problem for jets issuing from orifices of several different shapes. The problem is formulated in § 2 and then transformed into a form more suitable for numerical integration. In § 3, a numerical method, which we have used to integrate the problem outlined in § 2, is briefly described. This method appears to be new and it may be useful in solving other nonlinear free boundary-value problems. In particular, the authors are currently using this method to study the effects of surface tension on slender jets.

In § 4, we present the different orifice shapes for which our calculations were made. These shapes include the ellipse (which was a check on our numerical scheme), an egg-shaped cross-section, a square, a rectangle, and an equilateral triangle. We discuss these results in § 5.

2. Formulation of the problem

Let the velocity potential of the jet be denoted by $\Phi = \Phi(r, \theta, z; \epsilon)$ and let the shape of the free surface of the jet be described by $r = \mathscr{S}(\theta, z; \epsilon)$ (see figure 1). Here r, θ and z form the usual (non-dimensional) cylindrical co-ordinate system, with the positive z axis pointing vertically downward in the direction of gravity. The parameter ϵ, the slenderness ratio of the jet, is the ratio of a typical radius of the jet to a typical length along the jet and is defined precisely by Geer (1977*a*). The boundary conditions at the free surface are the kinematic condition of no flow through the surface and

Bernoulli's equation with constant pressure. For small values of ϵ, Geer (1977*a*) has shown that Φ and $\mathscr{S}$ are given by

$$\Phi = \tfrac{2}{3}(1+z)^{\frac{3}{2}} + \epsilon^2\phi(r,\theta,z) + O(\epsilon^3), \tag{2.1}$$

$$\mathscr{S} = S(\theta,z) + O(\epsilon), \tag{2.2}$$

where ϕ and S satisfy the conditions

$$\frac{\partial^2\phi}{\partial r^2} + \frac{1}{r}\frac{\partial\phi}{\partial r} + \frac{1}{r^2}\frac{\partial^2\phi}{\partial\theta^2} = -\tfrac{1}{2}(1+z)^{-\frac{1}{2}}, \quad z > 0, \quad 0 \leqslant r < S(\theta,z), \tag{2.3}$$

with

$$\frac{\partial\phi}{\partial r} - \frac{1}{S^2}\frac{\partial S}{\partial\theta}\frac{\partial\phi}{\partial\theta} = (1+z)^{\frac{1}{2}}\frac{\partial S}{\partial z} \tag{2.4}$$

and

$$\left(\frac{\partial\phi}{\partial r}\right)^2 + S^{-2}\left(\frac{\partial\phi}{\partial\theta}\right)^2 + 2(1+z)^{\frac{1}{2}}\frac{\partial\phi}{\partial z} = 0, \tag{2.5}$$

holding on $r = S(\theta,z)$. Equation (2.3) follows from Laplace's equation for the potential while equations (2.4) and (2.5) result from the substitution of the perturbation expansions (2.1) and (2.2) in the boundary conditions. Thus, we see that ϕ must satisfy the two-dimensional Poisson equation (2.3) in the cross-section of the jet, while equation (2.4) essentially prescribes the normal derivative of ϕ at the boundary of the cross-section. Equation (2.5) is the additional condition which is needed to determine the free surface.

To find ϕ and S, we transform the problem (2.3)–(2.5) into a form that is somewhat easier to deal with numerically. We first note that we can easily find a particular solution to (2.3) and consequently we write ϕ in the form

$$\phi = -\tfrac{1}{8}(1+z)^{-\frac{1}{2}}r^2 + \psi, \tag{2.6}$$

where ψ satisfies the homogeneous version of equation (2.3), i.e. Laplace's equation. Both ψ and S are presumed known at $z = 0$. We then introduce a new independent radial variable ρ, related to r by

$$\rho = \frac{r}{S(\theta,z)}. \tag{2.7}$$

Thus, r is stretched in a non-uniform manner, but the unknown boundary $r = S(\theta,z)$ is mapped onto the known boundary $\rho = 1$. We also define the new dependent variable $R(\theta,z)$ by

$$R(\theta,z) = \tfrac{1}{2}S(\theta,z)^2(1+z)^{\frac{1}{2}}. \tag{2.8}$$

In terms of the independent variables ρ, θ, and z, and the dependent variables $\psi(\rho,\theta,z)$ and $R(\theta,z)$, equations (2.4) and (2.5) can be written as

$$\frac{\partial R}{\partial z} = (1+\beta^2)\frac{\partial\psi}{\partial\rho} - \beta\frac{\partial\psi}{\partial\theta}, \tag{2.9}$$

$$4R\frac{\partial\psi}{\partial z} = (1+\beta^2)\left(\frac{\partial\psi}{\partial\rho}\right)^2 - \left(\frac{\partial\psi}{\partial\theta}\right)^2 - \frac{3}{4}\frac{R^2}{(1+z)^2}, \tag{2.10}$$

where

$$\beta = \frac{1}{S}\frac{\partial S}{\partial\theta} = \frac{1}{2}\frac{1}{R}\frac{\partial R}{\partial\theta}.$$

These equations hold for $\rho = 1$, $0 \leqslant \theta \leqslant 2\pi$, and $z > 0$. The differential equation (2.3) then becomes

$$(1+\beta^2)\frac{1}{\rho}\frac{\partial}{\partial\rho}\left(\rho\frac{\partial\psi}{\partial\rho}\right) - \frac{\partial\beta}{\partial\theta}\frac{1}{\rho}\frac{\partial\psi}{\partial\rho} + \frac{1}{\rho^2}\frac{\partial^2\psi}{\partial\theta^2} - 2\beta\frac{1}{\rho}\frac{\partial^2\psi}{\partial\rho\,\partial\theta} = 0, \tag{2.11}$$

$$0 \leqslant \theta \leqslant 2\pi, \quad 0 \leqslant \rho < 1, \quad z \geqslant 0.$$

As a consequence of equations (2.3)–(2.5), we find the integrability condition

$$\int_0^{2\pi} R(\theta, z)\, d\theta = \text{constant}, \tag{2.12}$$

which expresses the constant mass flux in the jet.

Thus, we seek solutions to equations (2.9)–(2.11) for ψ and R in the region

$$0 \leqslant \rho \leqslant 1, \quad z > 0.$$

Once ψ and R have been found, ϕ and S can be recovered using (2.6) and (2.8).

3. Method of solution

In this section we shall briefly describe the method we have devised to solve the problem formulated in § 2. A detailed discussion and analysis of the method, including motivation for the particular formulae used, will be presented elsewhere (see Strikwerda & Geer 1981).

Instead of attempting to solve the differential equation (2.11) subject to the auxiliary conditions (2.9)–(2.10) and (2.12) (as in a classical approach), we proceed in a different manner. To begin, we temporarily think of both ψ and R as functions of z and θ, defined only on the boundary $\rho = 1$. Then, in this context, we may regard equations (2.9)–(2.10) as a system of two nonlinear hyperbolic pseudo-differential equations for ψ and R, with z being the time-like variable and θ the spatial variable. These equations are hyperbolic because the first-order symbol of the linearized system has purely imaginary eigenvalues. They are 'pseudo'-differential equations because the operator $\partial/\partial\rho$ is a non-local operator on ψ, when considered as defined only on $\rho = 1$. However, the 'auxiliary' condition (2.11) which holds for $\rho < 1$ serves to define $\partial\psi/\partial\rho$ in terms of ψ and R on the boundary. Condition (2.12) is then a conservation law of the system.

The specification of R and ψ at $z = 0$ are the two initial conditions required by this initial-value problem. In all cases considered here ψ was initially zero which implies that $\partial R/\partial z$ is zero also, i.e. the jet is locally cylindrical at $z = 0$.

In order to obtain a numerical approximation to the solution of our problem formulated in this manner, we use a finite difference scheme defined on the grid points as follows:

$$\left.\begin{aligned} \theta_i &= (i-1)\,\Delta\theta, & i &= 1, \ldots, N, \\ \rho_j &= 1-(j-1)\,\Delta\rho, & j &= 1, \ldots, M, \\ z_n &= n\Delta z, & n &= 0, 1, 2, 3, \ldots, \end{aligned}\right\} \tag{3.1}$$

where $\Delta\theta = 2\pi/(N-1)$, $\Delta\rho = 1/(M-1)$, and Δz is chosen to satisfy appropriate stability and accuracy criteria. Note that $\theta_1 = 0$, $\theta_N = 2\pi$, $z_0 = 0$, $\rho_1 = 1$ and $\rho_M = 0$.

We then use the MacCormack scheme (MacCormack 1969) to solve equations (2.9)–(2.10). In particular, if we define the vector $\mathbf{w}(\theta, z)$ by $\mathbf{w} = (R, \psi)^T$, then equations (2.9)–(2.10) can be written as

$$\frac{\partial \mathbf{w}}{\partial z} = \mathbf{F}\left(z, \mathbf{w}, \frac{\partial \mathbf{w}}{\partial \theta}, \frac{\partial \psi}{\partial \rho}\right), \tag{3.2}$$

where the form of the vector $\mathbf{F}$ can be determined from the right-hand sides of (2.9)–(2.10). We employ the forward and backward difference operators, D_+ and D_-, respectively, defined by

$$\left.\begin{aligned} D_+ \mathbf{w}_i^n &= (\mathbf{w}_{i+1}^n - \mathbf{w}_i^n)/\Delta\theta, \\ D_- \mathbf{w}_i^n &= (\mathbf{w}_i^n - \mathbf{w}_{i-1}^n)/\Delta\theta, \\ \mathbf{w}_i^n &= \mathbf{w}(\theta_i, z_n). \end{aligned}\right\} \tag{3.3}$$

Then the forward–backward MacCormack scheme we use is given by the following two-step formula:

$$\tilde{\mathbf{w}}_i^{n+1} = \mathbf{w}_i^n + \Delta z \mathbf{F}(z_n, \mathbf{w}_i^n, D_+ \mathbf{w}_i^n, D_\rho \psi_i^n) \quad \text{predictor;} \tag{3.4}$$

$$\mathbf{w}_i^{n+1} = \tfrac{1}{2}\{\mathbf{w}_i^n + \tilde{\mathbf{w}}_i^{n+1} + \Delta z F(z_{n+1}, \tilde{\mathbf{w}}_i^{n+1}, D_- \tilde{\mathbf{w}}_i^{n+1}, D_\rho \tilde{\psi}_i^{n+1}\} \quad \text{corrector.} \tag{3.5}$$

Here $D_\rho \psi_i^n$ is an approximation to $\partial\psi/\partial\rho$ on $\rho = 1$ at $\theta = \theta_i$ and $z = z_n$. In order to maintain symmetry, the forward–backward MacCormack scheme is alternated with the backward–forward scheme, which uses backward differences in the predictor step and forward differences in the corrector step. Also it was found that the conservation law (2.12) was satisfied more closely when the quantity β in equations (2.9) and (2.10) was approximated as

$$D_\pm R_i^n/(R_i + R_{i\pm1}),$$

and this form was used in all the calculations given here.

The term $D_\rho \psi_i^n$ in (3.4) and (3.5) is computed by first solving for an approximation to the solution ψ of (2.11), with ψ_i^n specified on the boundary. The approximation is given by

$$\begin{aligned} &A_i^n \rho_j [\rho_{j-\frac{1}{2}}(\psi_{i,j-1} - \psi_{i,j}) - \rho_{j+\frac{1}{2}}(\psi_{i,j} - \psi_{i,j+1})]\,(\Delta\rho)^{-2} \\ &\quad - C_i^n \rho_j (\psi_{i,j-1} - \psi_{i,j+1})\,(2\Delta\rho)^{-1} + (\psi_{i+1,j} - 2\psi_{i,j} + \psi_{i-1,j})\,(\Delta\theta)^{-2} \\ &\quad - \rho_j \{B_{i+}^n [\psi_{i+1,j-1} - \psi_{i,j-1} - \psi_{i+1,j+1} + \psi_{i,j+1}] \\ &\quad + B_{i-}^n (\psi_{i,j-1} - \psi_{i-1,j-1} - \psi_{i,j+1} + \psi_{i-1,j+1})\}\,(2\Delta\rho\Delta\theta)^{-1} = 0. \end{aligned} \tag{3.6}$$

Here, $\psi_{i,j} = \psi(\rho_j, \theta_i, z_n)$, and

$$\left.\begin{aligned} B_{i\pm}^n &= (D_\pm R_i^n)/(R_i^n + R_{i\pm1}^n), \\ A_i^n &= 1 + \tfrac{1}{2}[(B_{i+}^n)^2 + (B_{i-}^n)^2], \\ C_i^n &= (B_{i+}^n - B_{i-}^n)/\Delta\theta. \end{aligned}\right\} \tag{3.7}$$

Equations (3.6) are solved by successive over-relaxation. Once $\psi_{i,j}^n$ is determined, the term $D_\rho \psi_i^n$ is computed as

$$D_\rho \psi_i^n = (3\psi_{i,1}^n - 4\psi_{i,2}^n + \psi_{i,3}^n)/2\Delta\rho, \tag{3.8}$$

which is a second-order one-sided approximation to $\partial\psi/\partial\rho$.

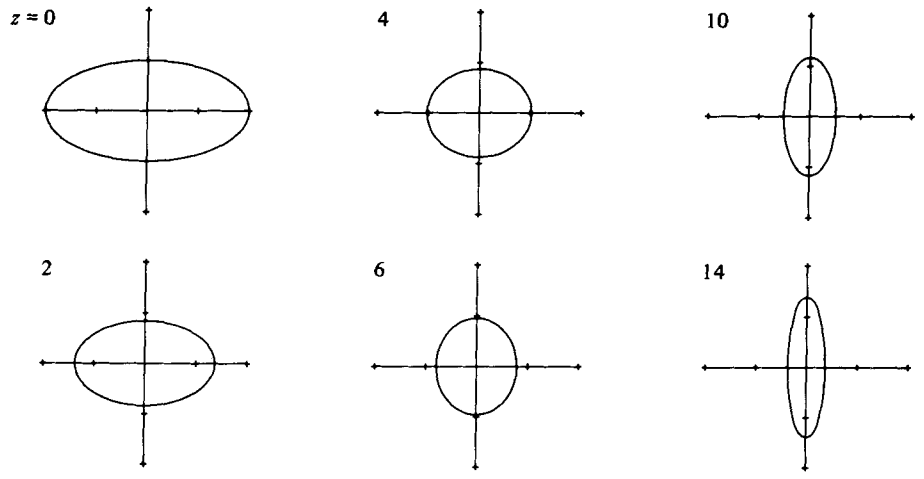

FIGURE 2. Cross-sectional shapes at several values of z for a jet with an initial shape of an ellipse.

Equations (3.1)–(3.8) describe our numerical scheme to solve the problem of § 2. The scheme has been shown to be second-order accurate in both θ and z (see Strikwerda & Geer 1981 for details).

4. Examples

Several examples of thin streams falling vertically through an orifice of a specified shape were calculated using the scheme outlined in the previous section. For each example the initial conditions were $\psi = 0$ and $R(\theta, z)$, i.e. $S(\theta, z)$, specified at $z = 0$. Note that the condition $\psi = 0$ at $z = 0$ corresponds to a jet that is emanating with a uniform velocity profile. Thus, in the notation of § 3, we set $\psi^0_{i,j} = 0$ and $R^0_i = R^0(\theta_i)$ at $z = 0$ where $R^0(\theta)$ was specified by one of the following:

(1) an ellipse, $R^0 = \frac{1}{2}(0{\cdot}25\cos^2\theta + \sin^2\theta)^{-1}$, where the semi-axes of the ellipse are 2 and 1 (figure 2);

(2) a square, $R^0 = \frac{1}{2}\min(\sec^2\theta, \operatorname{cosec}^2\theta)$, where the length of the side of the square is 2 (figure 3);

(3) a rectangle, $R^0 = \frac{1}{2}\min(\sec^2\theta, 4\operatorname{cosec}^2\theta)$, where 2 and 4 are the lengths of the sides of the rectangle (figure 4);

(4) an equilateral triangle, $R^0 = \frac{1}{2}\min_{l=0,1,2}\sec^2(\theta - \frac{2}{3}\pi l)$ where the length of the side of the triangle is $\sqrt{3}$ (figure 5);

(5) an egg-shape, which consists of a semi-circle of radius 1 joined with continuous tangent to a semi-ellipse with semi-minor axis 1 and semi-major axis 2 (figure 6);

(6) a 'sawed-off' ellipse, which consists of the same ellipse as in example 1, except that in the first and third quadrants the ellipse is replaced by a straight line segment so that the entire contour is continuous (figure 7).

For each example, the origin was located at the centre of mass of the shape, as required in the derivation of the basic equations (2.3)–(2.5) (see Geer 1977*a*). The corresponding figures show cross-sections of the jet at several values of z.

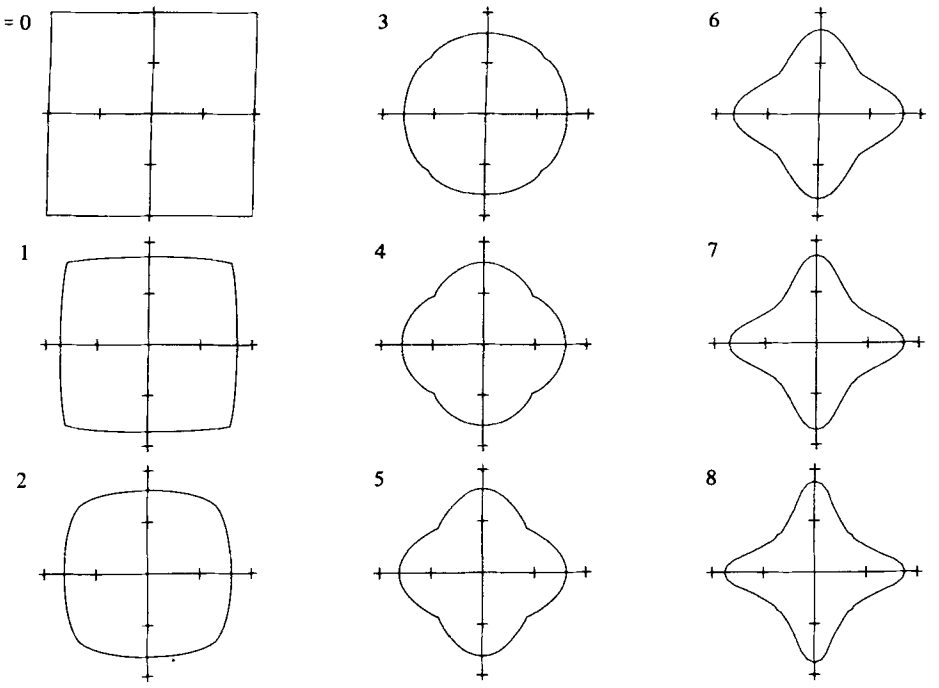

FIGURE 3. Cross-sectional shapes for a jet with an initial shape of a square with side of length 2.

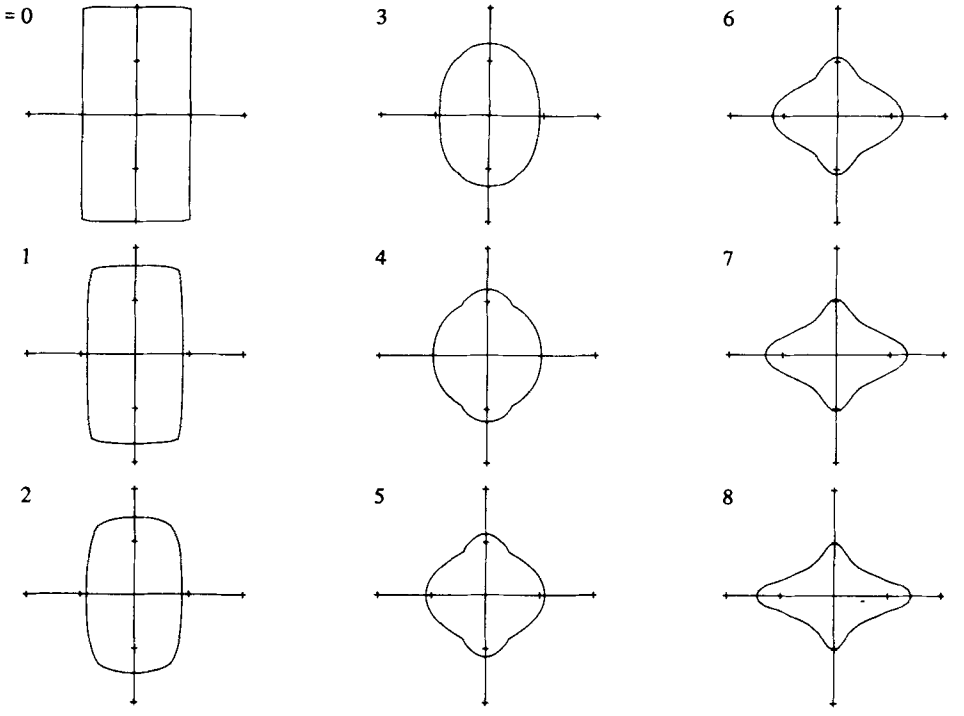

FIGURE 4. Cross-sectional shapes for a jet with the initial shape of a rectangle with sides of length 2 and 4.

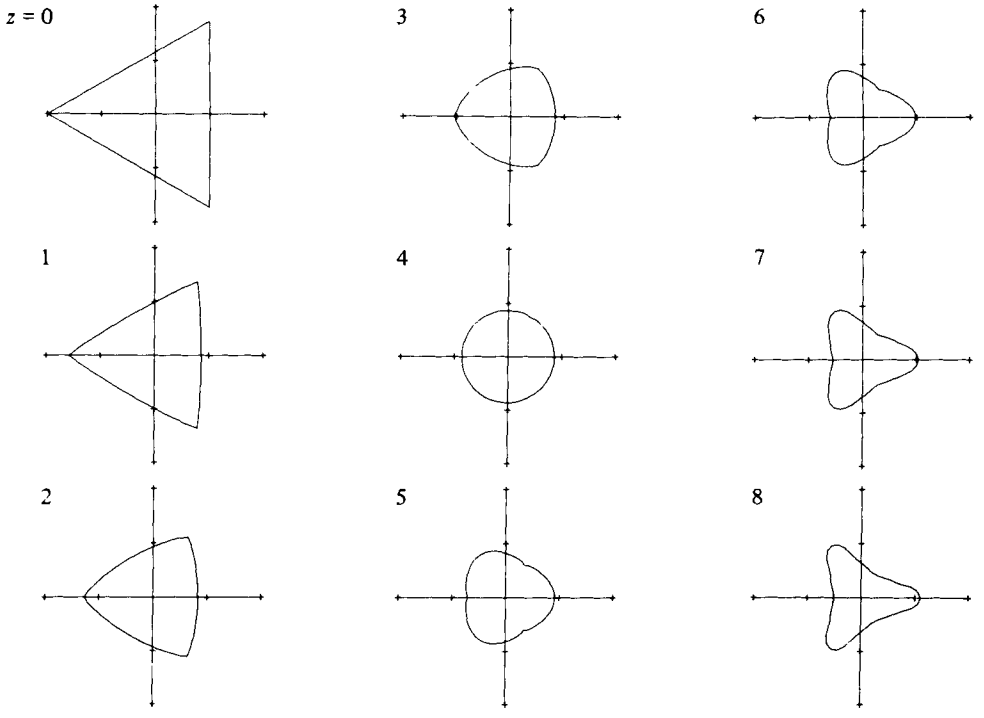

FIGURE 5. Cross-sectional shapes at several values of z for a jet with the initial shape of an equilateral triangle, with side of length $\sqrt{3}$.

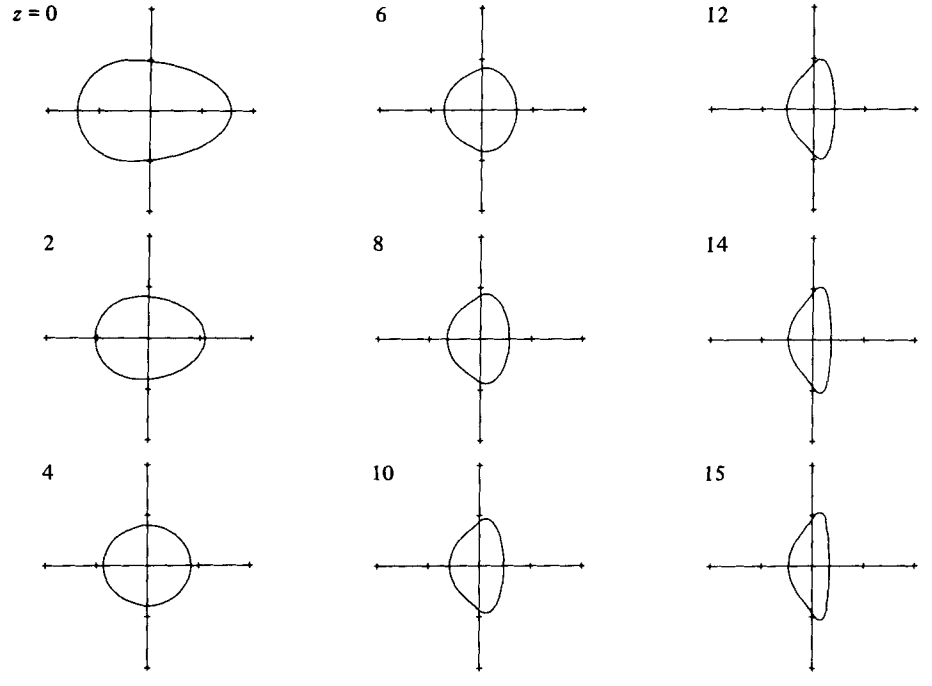

FIGURE 6. Cross-sectional shapes for a jet with an initial egg-shape formed by a semi-circle of unit radius and a semi-ellipse with semi-major axis of length 2.

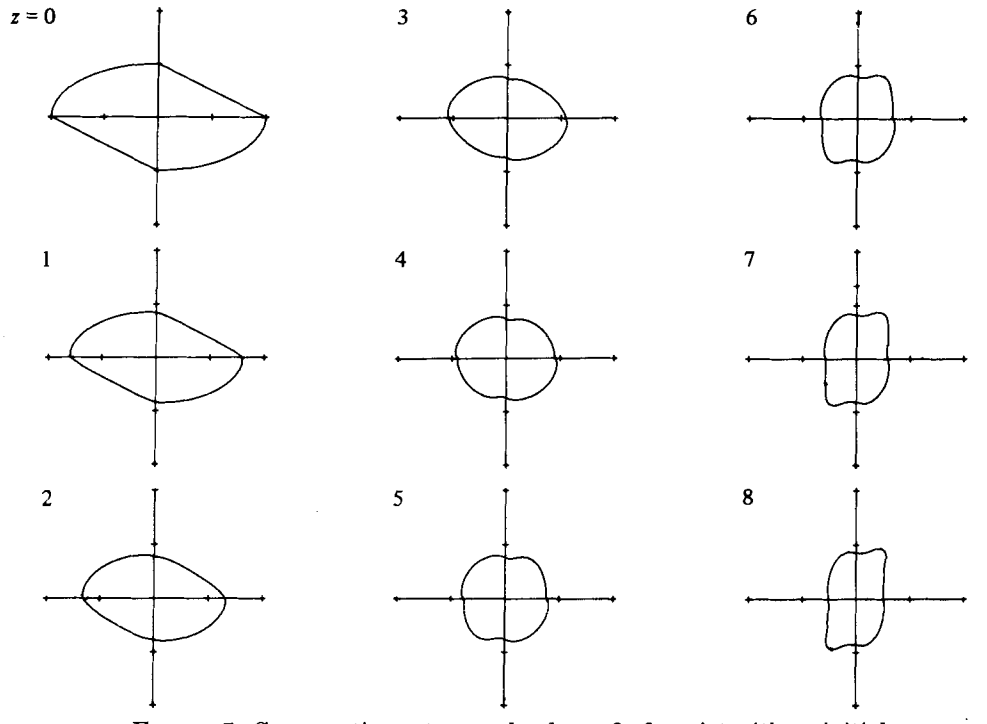

FIGURE 7. Cross-sections at several values of z for a jet with an initial cross-sectional shape in the form of a modified ellipse.

5. Discussion of the results

The primary purpose of the first example, the ellipse, was to check the accuracy of the numerical scheme. The numerical solution was compared with the analytic solution presented by Geer (1977*a*). The calculation of this analytic solution involved only the straightforward numerical integration of nonlinear ordinary differential equations, and consequently we assumed that this solution is known exactly.

Figure 2 shows the cross-sectional shape of the jet at various values of z. At $z = 0$, the ellipse has an aspect ratio of 2. As z increased, the shape of the jet became less eccentric, was nearly circular at about $z = 4{\cdot}9$, and then assumed an elliptical shape with the direction of the major and minor axes exactly interchanged with those of the original axes. The cross-sectional shape became more and more elongated as z increased. At $z = 14{\cdot}0$, the numerical solution with $N = 101$, $M = 31$, and $\Delta z = 0{\cdot}1$ agreed with the analytic solution to within 1 % relative error in the l^2- and l^1-norms, and to within 2 % relative error in the maximum norm.

In all of our examples the computations terminated when the outward moving portions became sufficiently elongated so that they could no longer be resolved adequately by the uniform grid used for the angular co-ordinate. The numerical break-up of the solution occurred soon after the last cross-section shown in each case. The conservation law (2.12) was satisfied to within 0·5 % relative error in all the cases shown here.

The next three examples had for initial shapes a square (figure 3), a rectangle (figure 4),

and an equilateral triangle (figure 5). The initial length of a side of the square was 2 units, the sides of the rectangle were 4 units and 2 units, and the side of the triangle was $\sqrt{3}$ units. (Thus the scale in figure 3 differs from that of the others by a factor of 2.) For these examples, for small values of z the cross-sectional shapes decreased in area, but maintained essentially the same shape. In particular the discontinuities in the slopes at the corners were propagated for some distance in z. For larger values of z the shape became non-convex as those portions of the surface that had been corners 'buckled-in'. Those portions of the surface that had originally been the sides formed the new extremities of the cross-sectional shape. For the case of the square and equilateral triangle the extremities all extended outward as z increased. For the case of the rectangle the major extremities extended outward and the minor extremities moved slowly inward. The numerical break-up of these cases occurred along these outward moving extremities as noted above.

We point out that these results are consistent with those of Bidone discussed by Rayleigh (1879) '... a vein issuing from an orifice in the form of a regular polygon, of any number of sides, resolves itself into an equal number of thin sheets, whose planes are perpendicular to the sides of the polygon' (see also Rayleigh 1945). Because of this qualitative agreement we feel that neglecting surface tension is justified for the case when inertial and gravitational forces predominate.

However, Rayleigh (1879) implies by his sketches that a jet emanating from an equilateral triangular orifice assumed at one point a hexagonal cross-section. Our calculations did not produce such a shape and we presume that this discrepancy is due to mistaken observations near the point where the cross-section was circular.

The cases with square and rectangular initial shapes were run with $N = 81$, $M = 31$, and $\Delta z = 0{\cdot}1$. The triangular shape was run with $N = 61$, $M = 31$, and $\Delta z = 0{\cdot}1$. In these examples, the value of N was chosen so that a grid point would be at or very near the corner of the original shape.

The two final examples are shown in figures 6 and 7. The previous examples involved shapes with several planes of symmetry. These last two examples treat an egg-shape with only one plane of symmetry, and a modified elliptical shape, with no plane of symmetry.

The initial egg-shape of the fifth example had a continuous tangent, and the resulting jet did not develop any discontinuities. As in the earlier examples, the points on the boundary that were initially farthest from the origin moved toward the origin more rapidly than other points. The jet had a nearly circular cross-section at $z = 4{\cdot}0$, and then bulged out as it began to form a thin sheet in the direction perpendicular to the long direction of the initial shape. Note that the sheet formed on the side that had been the long end or elliptical portion of the egg-shape and a more compact mass remained near the origin on the side that had been the short end or circular portion of the original shape. For this case $N = 101$, $M = 31$, and $\Delta z = 0{\cdot}1$.

The last example, which used the modified elliptical shape for the initial condition, had discontinuities in the tangent (figure 7). These discontinuities were not as large as those for the square, rectangle, and triangle, and they seemed to disappear sooner. As in the other examples, the portions of the boundary that were initially farthest from the origin moved inward most rapidly. The jet was most nearly circular in cross-section at about $z = 4$. We observe that the outward moving sheets that began to form appeared to be moving in the direction perpendicular to the straight sides of the original cross-

section. However, the solution has not been integrated far enough in z to determine this angle accurately. For this case $N = 81$, $M = 31$, and $\Delta z = 0{\cdot}1$.

We note that the two examples which had a continuous tangent in the initial shape, i.e. the ellipse and the egg-shape, could be integrated farther in z than the other examples (typically to $z = 14$). Although these two examples did have the largest values of N, i.e. 101, the examples with a discontinuous tangent could not be integrated up to $z = 12$, even with $N = 101$. Thus it appears that the discontinuities in the tangent cause the jets to produce narrower sheets of fluid more rapidly than would be the case with a smooth jet. Of course, since each of these jets had a different mass-flow rate and quite dissimilar profiles, it is difficult to quantify this conclusion.

These examples illustrate some of the prominent geometric features of jets for which inertial and gravitational forces dominate. They also show that the method of solution is applicable to a wide variety of jet orifices.

The first author was partially supported by the Research Foundation of S.U.N.Y. under Contract no. 240-6115A and partially supported under N.A.S.A. Contract no. NAS1-14101. The research of the second author was supported under N.A.S.A. Contract no. NAS1-14101 while he was in residence at ICASE, NASA Langley Research Center, Hampton, VA 23665.

REFERENCES

GEER, J. F. 1977*a* Slender streams with gravity: Outer asymptotic expansions I. *Phys. Fluids* **20**, 1613–1621.

GEER, J. F. 1977*b* Slender streams with gravity: Outer asymptotic expansions II. *Phys. Fluids* **20**, 1622–1630.

GEER, J. F. & KELLER, J. B. 1979 Slender Streams. *J. Fluid Mech.* **93**, 97–115.

GREEN, A. E. 1977 On the steady motion of jets with elliptical sections. *Acta Mech.* **26**, 171–177.

KELLER, J. B. & GEER, J. F. 1973 Flows of thin streams with free boundaries. *J. Fluid Mech.* **59**, 417–432.

MACCORMACK, R. W. 1969 The effect of viscosity in hypervelocity impact cratering. *A.I.A.A. Hypervelocity Impact Conf., A.I.A.A. Paper* no. 69–354.

RAYLEIGH, LORD 1879 On the capillary phenomena of jets. *Proc. Roy. Soc.* **29**, 71–97.

RAYLEIGH, LORD 1945 *The Theory of Sound*, 2nd edn. Dover.

STRIKWERDA, J. C. & GEER, J. F. 1981 A numerical method for computing the shape of a vertical slender jet. *S.I.A.M. J. Sci. & Stat. Comp.* (to appear).

TUCK, E. O. 1976 The shape of free jets of water under gravity. *J. Fluid Mech.* **76**, 625.